IV International Conference on Simulation for Additive Manufacturing
Sim-AM 2023
E. Rank and S. Kollmannsberger (Eds)

NUMERICAL INVESTIGATION OF PROPERTIES OF CHIRAL STRUCTURES WITH ARTIFICAL STRUCTURAL ANISOTROPY

SHUN NOGUCHI* AND KUNIHARU USHIJIMA†

*Graduate School of Engineering, Tokyo University of Science
6-3-1 Niijuku, Katsushika-ku, 1258585 Tokyo, Japan
e-mail: 4522537@ed.tus.ac.jp

†Tokyo University of Science
6-3-1 Niijuku, Katsushika-ku, 1258585 Tokyo, Japan
e-mail: kuniharu@rs.tus.ac.jp - Web page: http://www.rs.tus.ac.jp/kuniharu/

Key words: Numerical simulations, Natural frequency, Additive Manufacturing (AM)

Abstract. The dynamic vibration response of sandwich beams with an anti-tetra-chiral lattice as a lightweight sandwiched core have been studied by using a nonlinear finite element analysis (FEA). Since the anti-tetra-chiral structure has a weak shear stiffness, its vibration response is strongly affected by the shear deformation. In our calculation, a 3-point bending flexural test was conducted for calculating the effective shear stiffness as well as the effective Young's modulus of the chiral core. The natural frequency of the sandwich beam has been calculated by FEA, and predicted by using the Rayleigh-Ritz method, assuming that the sandwich beam is composed of composite continuum materials with equivalent Young's modulus and shear modulus. Moreover, the natural frequency and damping ration of the sandwich beam produced by a 3D printer bas been measured through a vibration test, and compared with numerical results in order to clarify the effectiveness of the chiral sandwich beam as a mechanical component.

1 INTRODUCTION

A chiral structure is composed of asymmetric unit-cells that are in a mirror-image relationship and cannot be overlapped. The structure can be found in many other objects in nature, and applied in many scientific fields, including physics, biology, and chemistry. Also, due to the rapid development of additive manufacturing technology, sandwich structures with chiral core can be easily created, and many research papers regarding the mechanical response of these structures has been published[1][2]. For example, Davood et al. have investigated the elastic properties of chiral, anti-chiral and hierarchical honeycombs based on a simple energy-based approach, and proposed theoretical equations for calculating the equivalent material properties[1]. On the other hand, industrial developments have raised issues related to vibration characteristics, and serious accidents such as train derailments and building damage would occur due to the resonance phenomenon that occurs when the natural frequency of an object matches the frequency of an external source. Therefore, a precise prediction and controlling of natural frequencies as well as enhancing the effect of damping vibrations becomes important in the design

of machines and buildings. The vibration behavior of chiral structure has also been studied by some researchers, but most of their work is based on experiments, and there are few reports on the prediction of natural frequencies or the assessment of damped vibrations by numerical analyses or theoretical investigations[3].

In this paper, we proposed an analytical model to predict the natural frequencies of sandwich beams with anti-tetra-chiral lattice based on the Rayleigh-Ritz method, and discussed the effectiveness of the analytical investigation by comparing with numerical results obtained by a nonlinear finite element analysis (FEA). In addition, the natural frequency as well as the damping ratio of the chiral sandwich beam produced by a 3D printer were measured in order to investigate the effectiveness of the chiral sandwich beam as a mechanical component.

2 THEORY AND ANALYTICAL METHOD

2.1 Analytical model

Figure 1 and 2(a)(b) show a schematic of anti-tetra-chiral, auxetic structures investigated in this study. The unit cell consists of a beam and a cylinder element, defined as a support and a ligament element (see Fig.2(b)). The dynamic vibration response including the structural damping have been investigated by using a commercial nonlinear finite element analysis software, COMSOL Multiphysics 6.0.

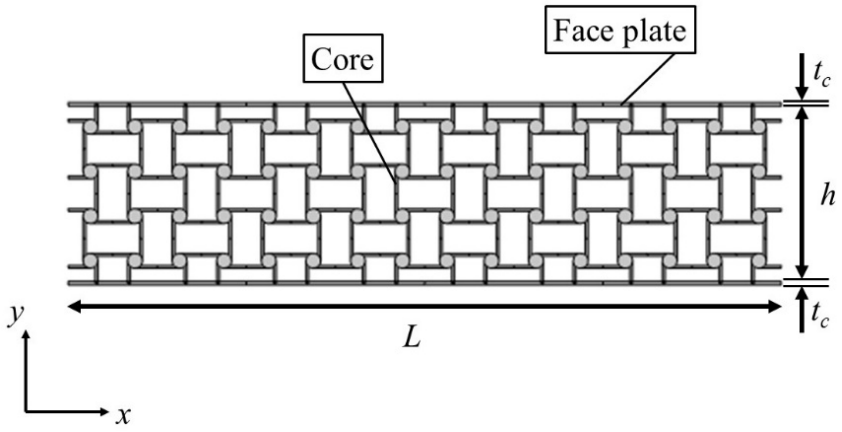

Figure 1: Cantilever sandwich beam with anti-tetra-chiral core

In this study, we have prepared three kinds of anti-tetra-chiral samples under the same relative density ρ. The details of geometrical parameters are shown in Table 1.

2.2 Mechanical properties of anti-tetra-chiral structures

In our calculation, the deformation of the anti-tetra-chiral under in-plane loading was assumed to be a ligament bending, and the mechanical properties are investigated by using the strain energy analysis in consideration with Euler-Bernoulli beam theory[4]. The geometrical parameters, t, l, and r, represent the ligament width, ligament length and support radius, respectively. Following the Davood et al's work[1], the in-plane mechanical properties of anti-

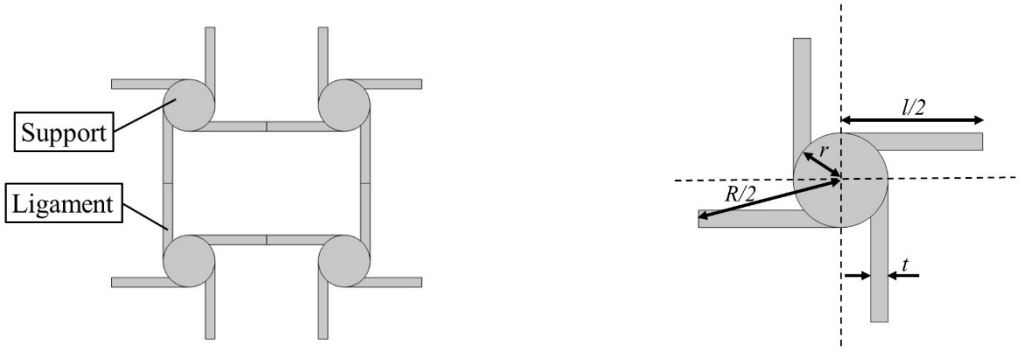

(a) Core **(b)** Unit cell

Figure 2: Schematic of anti-tetra-chiral structure

Table 1: Dimension parameter

	Model		
	1	2	3
Model ratio r/R [-]	0.100	0.158	0.200
Support length r [mm]	1.22	2.00	2.62
Cell length R [mm]	12.2	12.6	13.1
Ligament length l [mm]	12.0	12.0	12.0
Ligament width t [mm]	1.00	0.734	0.380

tetra-chiral structure can be expressed as follows:

$$E^* = \frac{t/l}{1 + 6(r/l)^2/(t/l)^2} E_s, \tag{1}$$

for equivalent Young's modulus, and

$$G^* = 0.5 \left(\frac{t}{l}\right)^3 E_s, \tag{2}$$

for equivalent shear modulus, and

$$\nu_{xy} = -\frac{\varepsilon_y}{\varepsilon_x} = \frac{-6(r/l)^2}{6(r/l)^2 + (t/l)^2}, \tag{3}$$

for equivalent Poisson's ratio. These values would be used for predicting the vibration response of the anti-tetra-chiral sandwich panel.

2.3 Effective shear modulus G^*

It is widely known that the effective shear modulus, G^*, derived by Eq.(2), is only applicable for square shape (L=h), and not applied for rectangle one ($L \neq h$) [4]. Following the Yamashita et al's work, we have prepared another FE model for 3-point bending test, and calculated the effective Young's modulus E^* and the effective shear modulus G^* of the chiral structure. The details of the numerical procedure was given in [4], and the dependence of the model aspect ratio L/h on these modules, E^* and G^*, would be discussed in Section 3.1.

2.4 Calculation of natural frequency based on the Rayleigh-Ritz method [5]

In this section, the prediction procedure for natural vibration frequencies of chiral-cored sandwich beams is introduced. the preduction scheme is based on the Reyleigh-Ritz method, and the following assumptions were considered;

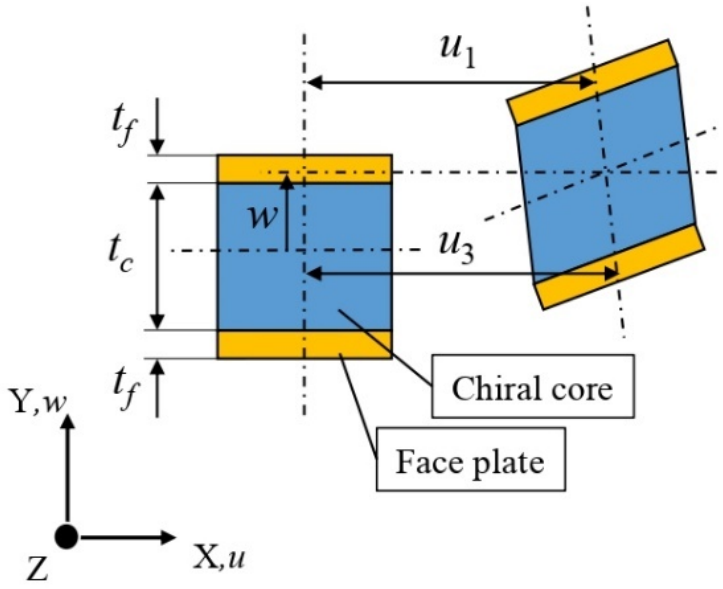

Figure 3: Schematic of displacement field of three-layered sandwich beam with chiral core

- The shear strain in faceplates is negligible
- The longitudinal direct stress in the core is negligible
- The transverse displacement at all points of the cross-section is constant

The strain energy stored in the face plates and the chiral core can be expressed by the following equation:

$$\begin{aligned} U &= U_f + U_c \\ &= \frac{G_c^* b(t_c+t_f)^2}{2t_c}\int_0^L \left(\frac{\partial w}{\partial x}\right)^2 dx + \frac{E_s b t_f^3}{12}\int_0^L \left(\frac{\partial^2 w}{\partial x^2}\right)^2 dx + \frac{G_c^* b}{2t_c}\int_0^L (u_1^2+u_3^2)dx \\ &\quad + \frac{E_s b t_f}{2}\int_0^L \left(\frac{\partial u_1}{\partial x}\right)^2 dx + \frac{E_s b t_f}{2}\int_0^L \left(\frac{\partial u_3}{\partial x}\right)^2 dx - \frac{G_c^* b}{t_c}\int_0^L u_1 u_3 dx \\ &\quad + \frac{G_c^* b(t_c+t_f)}{t_c}\int_0^L (u_3-u_1)\frac{\partial w}{\partial x}dx. \end{aligned} \tag{4}$$

Here, subscripts f and c denote the face plate and the chiral core, respectively. Also. u_1 and u_3 represent the displacements for the top and bottom face plates along the x-direction, and w

represents the displacement at the center of the chiral core along the y-direction. The kinetic energy of the chiral cored sandwich beam T can be given by:

$$\begin{aligned} T &= T_x + T_y \\ &= \frac{b\omega_n^2}{2}\rho_s t_f \int_0^L \left(u_1^2 + u_3^2\right) dx + \frac{b\omega_n^2}{2}\left(\rho_c t_c + 2\rho_s t_f\right) \int_0^L w^2 dx. \end{aligned} \tag{5}$$

Now, Hamilton's principle can be applied in order to calculate the natural frequency of the beam by using Eq.(4) and (5). The principle is expressed as follows:

$$\delta \int_{t_1}^{t_2} (T - U)\, dt = 0, \tag{6}$$

where δ is the variational operator and t_1 and t_2 define the time interval for a single period.

The displacements w, u_1 and u_3 are assumed to be expressed in terms of a series of admissible functions as follows:

$$w(x,t) = \widetilde{w}(x)e^{j\omega_n t}, u_1(x,t) = \widetilde{u_1}(x)e^{j\omega_n t}, u_3(x,t) = \widetilde{u_3}(x)e^{j\omega_n t}, \tag{7}$$

here, $j^2 = -1$, and ω_n denotes the natural frequency($= 2\pi/(t_2 - t_1)$). Also, it is assumed that the functions $\widetilde{w}$, $\widetilde{u_1}$ and $\widetilde{u_3}$ can be expressed as a series of polynomials as follows:

$$\widetilde{w}(x) = \sum_{i=1}^{N} A_i f_i(x), \widetilde{u_1}(x) = \sum_{i=1}^{N} B_i g_i(x), \widetilde{u_3}(x) = \sum_{i=1}^{N} C_i g_i(x), \tag{8}$$

here, $f_i(x)$ and $g_i(x)$ are the polynomial function which satisfy the geometrical boundary conditions for a given problem. For example, as for the clamped-free beam problem, the fuctions $f_i(x)$ and $g_i(x)$ can be written by:

$$f_i(x) = g_i(x) = x^{i+1}. \tag{9}$$

Also, N represents the number of terms in the series.

Here we have introduced the potential V as follows:

$$V = \frac{\omega_n}{\pi} \int_{t_1}^{t_2} (T - U)\, dt. \tag{10}$$

In order to solve Eq.(6), the following equation must be satisfied:

$$\frac{\partial V}{\partial A_i} = \frac{\partial V}{\partial B_i} = \frac{\partial V}{\partial C_i}. \tag{11}$$

Substituting Eqs.(7), (8) into Eqs.(4), (5), (6) and (11), the simultaneous linear equations in $3N$ unknowns A_i, B_i and $C_i (i = 1, 2, ..., N)$ can be given as follows:

$$(\boldsymbol{D} - \omega_n^2 \boldsymbol{F})\boldsymbol{x} = 0, \tag{12}$$

where, $\boldsymbol{x} = (A_1, A_2, \cdots, A_N, B_1, B_2, \cdots, B_N, C_1\ C_2, \cdots, C_N)^T$ is unknown paratemers, and D and F are symmetric and diagonal matrix, respectively. The condition in which Eq.(12) does not have trivial solutuion for $\boldsymbol{x}$, can be written as:

$$det(\boldsymbol{D} - \omega_n^2 \boldsymbol{F}) = 0. \tag{13}$$

By calculating Eq.(13), n-th order natural frequency of chiral sandwich beam ω_n can be obtained. Finally, the frequency $f_n (= \omega_n/(2\pi))$ of the beam can be calculated.

2.5 Experimental set-up

In this study, two types of chiral sandwich specimens with different beam length L and height h were manufactured by using a Stereolithography (SLA) based 3D printer (Form3, Formlab Ltd.). The material used in this study was a light curable resin, with elastic modulus E_l=4.7 GPa, density ρ=1179.5 kg/m^3, and poisson's ratio ν =0.35. Also, regarding the modeling dimensions, the following values were applied: the thickness of the ligament t=0.5 mm, the support length r=0.667 mm, the cell length R=4.22 mm and the ligament length l=4.00 mm. Moreover, the depth in the z-direction was set to 15 mm. Figure 4(a)(b) show photographs of manufactured specimens attached with strain gages. Free vibration tests were conducted under impulse load, and the natural frequencies and the damping ratio were measured by the change in electrical resistance.

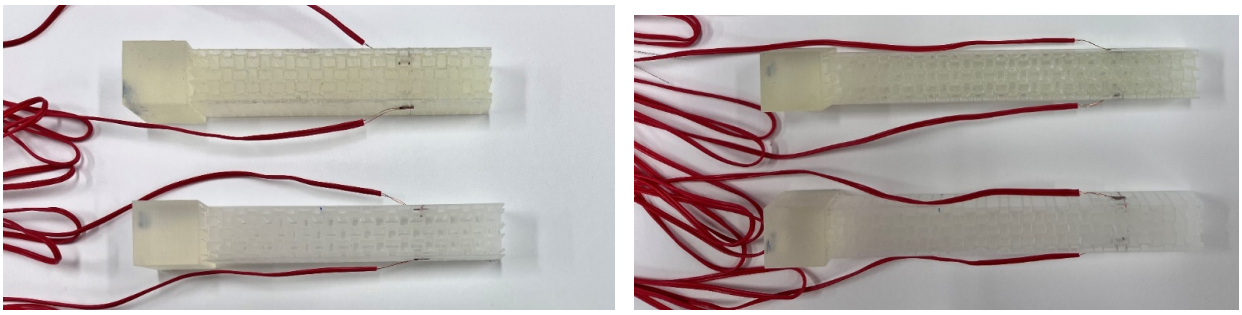

(a) beam's length-to-thickness ratio L/h=6.0 **(b)** beam's length-to-thickness ratio L/h=8.0

Figure 4: Photograph of actural specimen made of curable resin fabricated by 3D printer

3 RESULT AND DISCUSSION

3.1 Equivalent elastic moduluses, E^* and G^*

In this section, the influence of the aspect ratio L/h and the ligament ratio r/R on these effective modules, E^*, G^*, were investigated. Figure 5(a)(b) show deformed shapes of an anti-tetra-chiral unit cell subjected to uniaxial tension and shear load. Figure 6(a) shows comparisons of equivalent Young's modulus, E^*, for some cases of the ligament ratio r/R and the aspect ratio L/h obtained by FEA. As can be found from Fig.6(a) that the modulus E^* keeps a constant value regardless of the scale of L/h, and increases as the ratio r/R decreases. Also, these values obtained by FEA agree well with analytical prediction obtained by Eq.(1).

On the contrary, as for the equivalent shear modulus, G^*, it is anticipated that the modulus depends significantly on the aspect ratio L/h of the beam. Figure 6(b) shows the variation of the equivalent shear modulus obtained by FEA with beam's aspect ratio L/h. Also in this figure, the results for three kinds of the ratio r/R at the ligament part were plotted and compared with the analytical results obtained by Eq.(2). When the ratio L/h equals to 1, the result obtained by FEA agrees well with analytical prediction. Also, as the ratio L/h increases, the value of the modulus rises and drops gradually and converges to a constant value. In other words, there are mainly three regions.

Region (a): The modulus G^* increases rapidly as the aspect ratio L/h reaches 2.

Region (b): The modulus G^* decreases around the aspect ratio of 10 and reach an extreme value.

Region (c): The modulus G^* converges to a constant value.

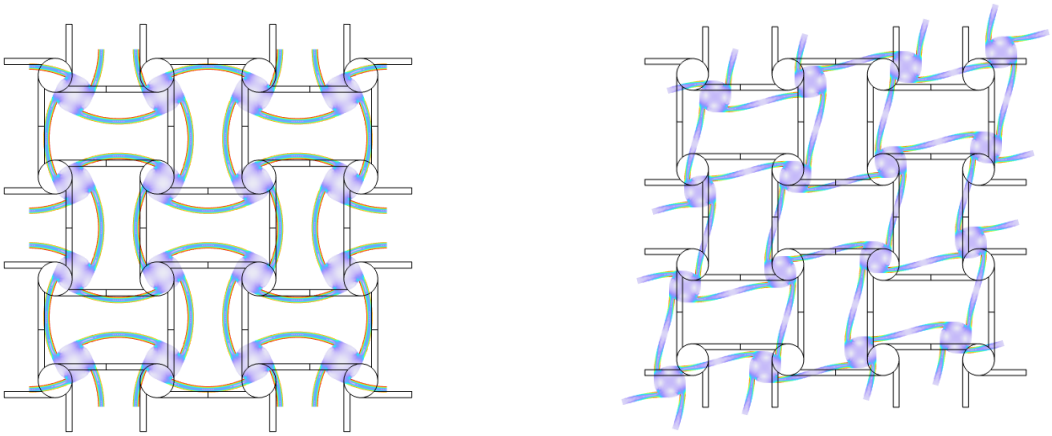

(a) subjected to uniaxial compressive load **(b)** subjected to shear load

Figure 5: Deformed shape of a chiral unit model

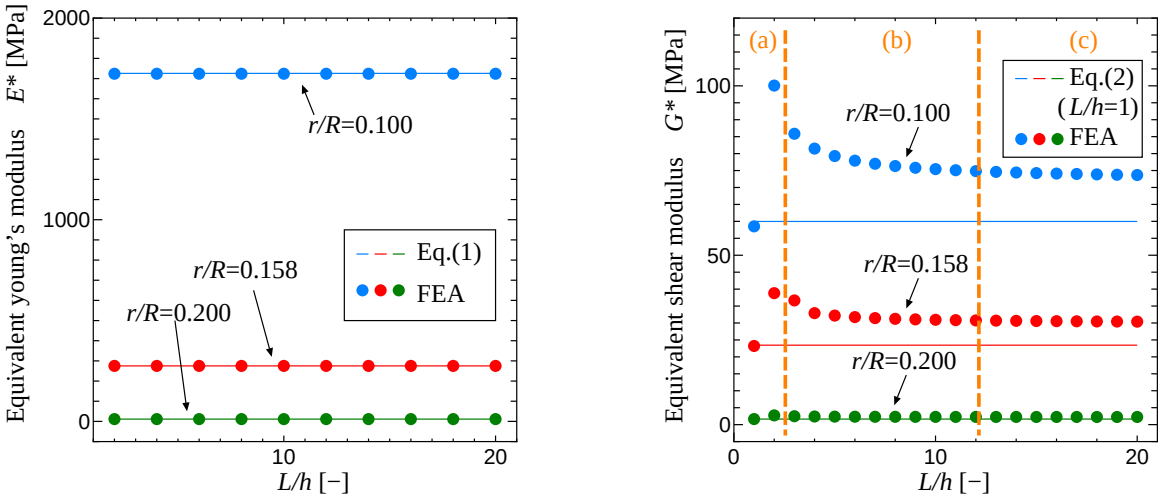

(a) effective Young's modulus E^* **(b)** effective shear modulus G^*

Figure 6: Effects of beam geometries on the effective elasitic modules E^* and G^*

3.2 Vibration response

Figure 7(a)-(d) show the first order vibration mode for a chiral-cored sandwich beam with different aspect ratio L/h=4.0, 8.0, 14 and 20. Here the ratio of the ligament part r/R is 0.158. It can be seen from these figures that as the aspect ratio L/h increases, the dominant

deformation mode shifts from shear in a chiral core to a bending of a whole beam. Figure 8 shows variations of the fritst order natural frequency f_1 with the aspect ratio L/h for the sandwich beams with different ligament ratio r/R. In this figure, marks show numerial results obtained by FEA, and curves show predictions derived from Eq.(13). Since the effective shear modulus G^* depends strongly on these ratios, r/R and L/h, the natural frequencies obtained by FEA also vary with these ratios. However, the analytixal predictions obtained by Eq.(13) agree well with FE results regardless of the values of L/h and r/R.

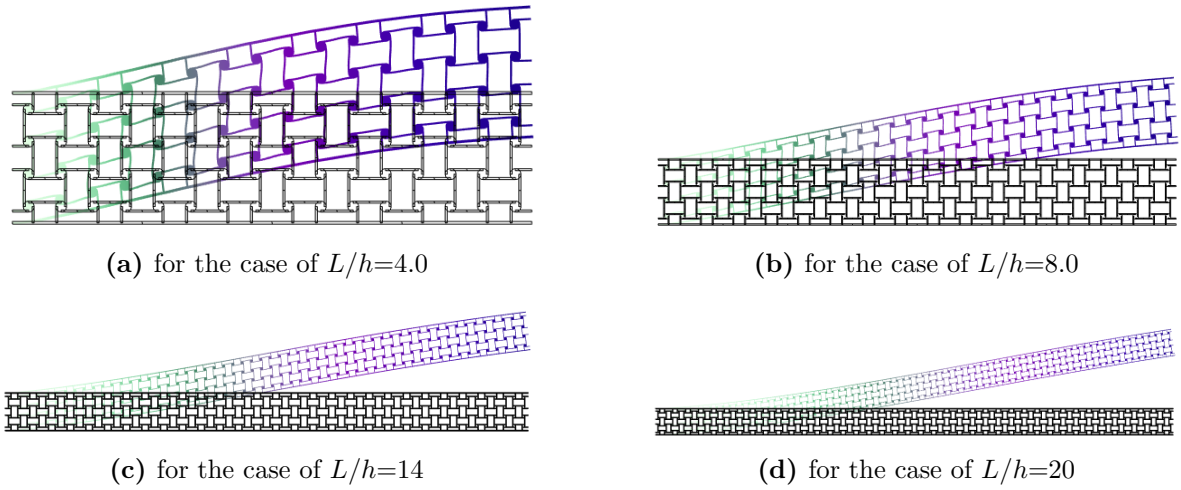

(a) for the case of L/h=4.0

(b) for the case of L/h=8.0

(c) for the case of L/h=14

(d) for the case of L/h=20

Figure 7: Comparisons of deformed shape of the first order vibration mode for chiral-cored sandwich beams with the same ratio r/R=0.158 at the ligament part

Figure 9(a) and (b) show an example of undeformed and deformed shape during vibraion of the chiral-cored sandwich beam with ratios r/R=0.158, L/h=8.0. Each colored rectangle represent the corresponding unit-cell before and after the movement. The size of the area of each rectangle can be calculated from the positions of the four surrounding points. In this study, the size of the area for all cells in a beam were measured from FE results, and calculated the area ratio $\tilde{S}$ determined by the following equation.

$$\tilde{S} = \frac{\text{(cross-sectional area after deformation)}}{.}\text{(cross-sectional area before deformation)} \quad (14)$$

This parameter $\tilde{S}$ indicates how much the shear deformation is dominant in a beam. Figure 10 shows the variation of the area ratio $\tilde{S}$ for some cases of r/R with beam's aspect ratio L/h. As can be found from Figure 10 that when the beam is relatively short, for instance, the aspect ratio L/h is less than 10, the area ratio $\tilde{S}$ deviates from 1. This tendency becomes signigficant for the larger value of r/R, since the effective shear stiffness G^* decreases as the ratio r/R increases. In this region, it can be understood that a shear observed in a chiral core is a dominant deformration. On the contrary, when the beam is sufficiently long, the ratio $\tilde{S}$ is almost equals to 1 regardless of the ratio r/R at the ligament part. It can be concluded that a bending of a whole beam is a dominant deformration in this region,

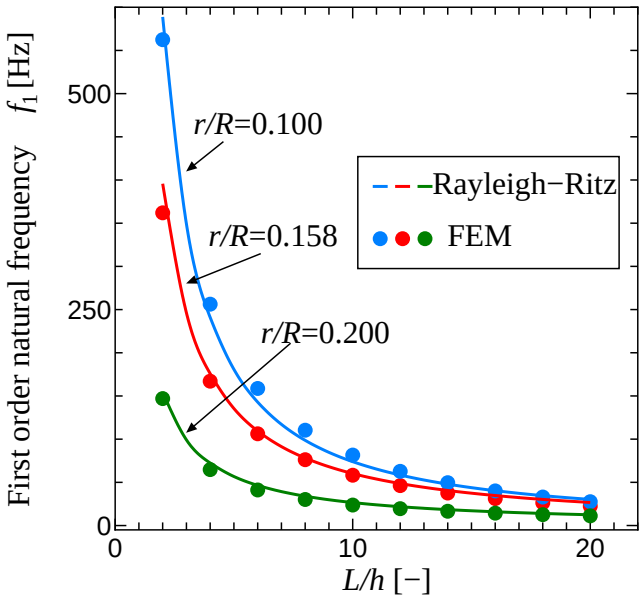

Figure 8: Effects of beam geometries on the first order natural frequency f_1

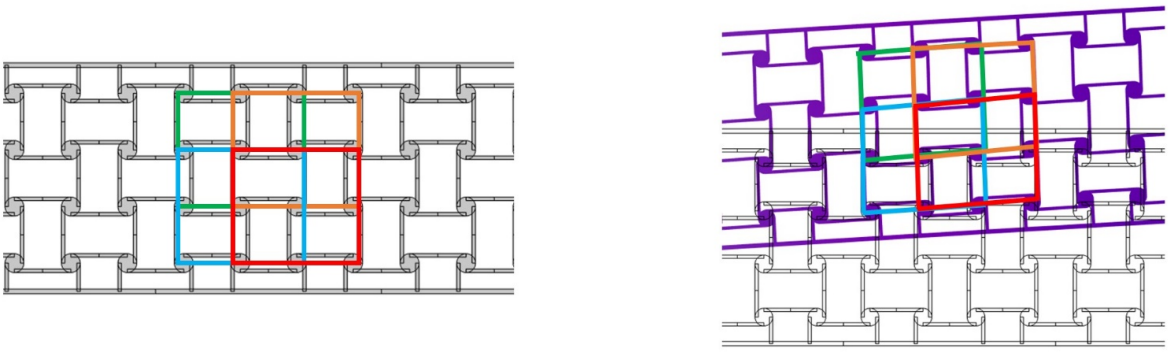

(a) undeformed shape **(b)** deformed shape

Figure 9: Comparison of undeformed and deformed shape of the chiral-cored sandwich beam under the condition of r/R=0.158 and L/h=8.0

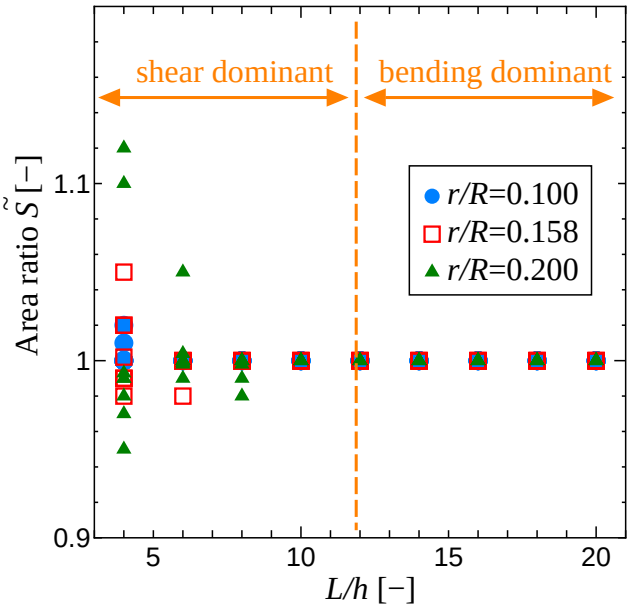

Figure 10: Variation of the area ratio $\tilde{S}$ with beam's aspect ratio L/h

3.3 Observation of vibration response

Figure 11(a)(b) show the variation of the voltage measured from the strain gages with the observation time for two specimens with different aspect ratio, $L./h$=6.0 and 8.0. It can be found in Fig.11 that the strong damping response was observed. The vibration experiment was condacuted three times for each specimen. Table 2 shows comparisons of the natural frequency measured by experiment and numeraical results obtained by FEA. As can be seen in Table 2 that these values show a similar trend, but with quantitative errors. The main cause of such discrepancy would lilely lie in the following two points. Firstly, it is anticipated that there are several close eigenfrequency modes exist. Figures 12(a)(b) and 13(a)(b) show the in-plane and out-of-plane vibration modes for sandwich beams with L/h =6 and 8 calcultated by FEA. As can be found that the value of eigenfrequency for out-of-plane mode is always smaller than that for in-plane mode. Secondly, it is anticipated there are unexpected irregularities in shape in a real specimen. Figure 14(a)(b) show the actural specimens. It can be seen that there is a upward slewing was observed for both specimens. Such a geometial imperfection would cause the error. In the next work, we must design sufficient supports and investigate appropriate UV condition for drying in order to minimize the occerence of geometrical imperfection.

Table 2: Comparisons of 1st order natural frequency f_1 of the chiral-cored sanwich beams with L/h=6.0 and 8.0 observed by experiment with FE results

aspect ratio	Experiment [Hz]				FEA [Hz]
L/h	No.1	No.2	No.3	Ave.	—
6.0	263.1	251.5	261.8	257.9	334.6
8.0	164.7	166.8	168.0	160.4	212.2

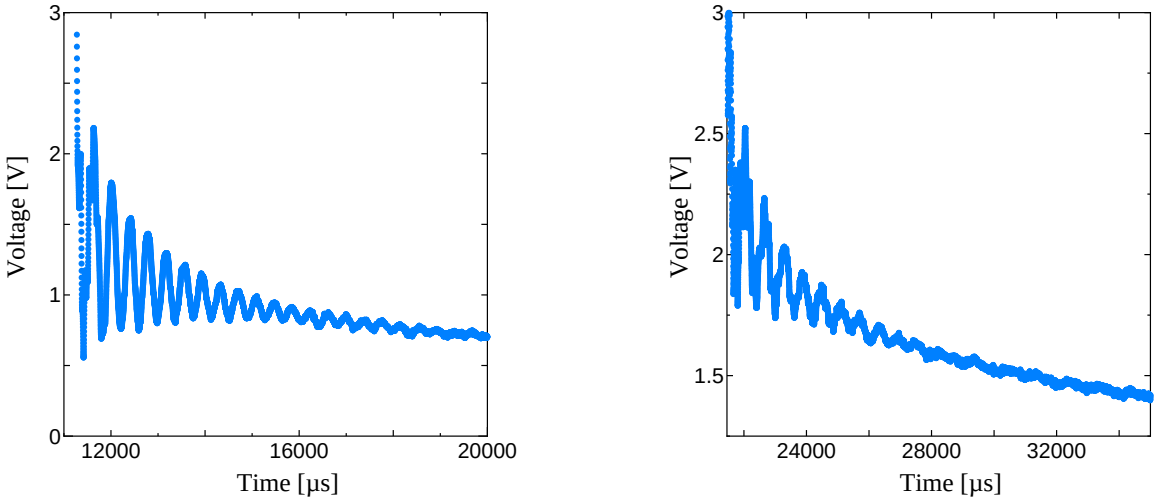

(a) for the case of L/h=6.0 **(b)** for the case of L/h=8.0

Figure 11: Comparisons of damping waveform of chiral-cored sandwich beams

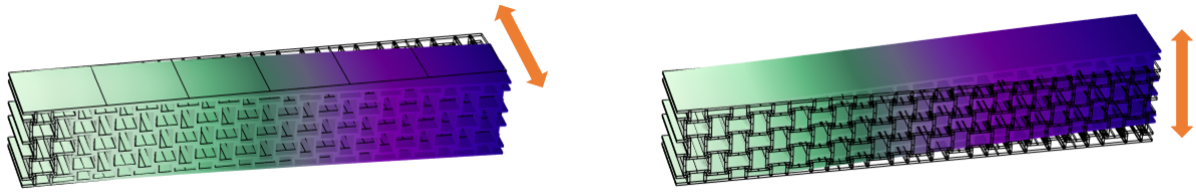

(a) out-of-plane mode (freq.=317.1 Hz) **(b)** in-plane mode (freq.=349.6 Hz)

Figure 12: Comprarisons of eigenequencies of the chiral-cored sanwich beams with L/h=6.0

(a) out-of-plane mode (freq.=179.3 Hz) **(b)** in-plane mode (freq.=223.3 Hz)

Figure 13: Comprarisons of eigenequencies of the chiral-cored sanwich beams with L/h=8.0

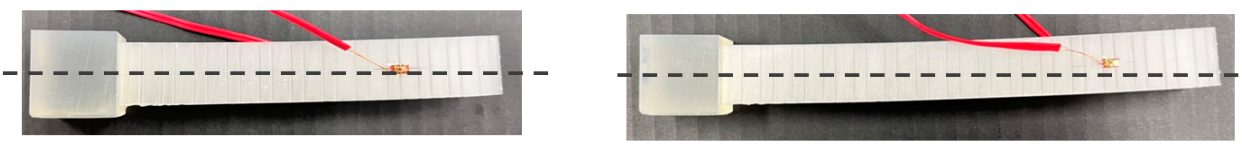

(a) for the case of L/h=6.0 **(b)** for the case of L/h=8.0

Figure 14: Observed geometical imperfection in 3D-printed sandwich beams

4 CONCLUSIONS

In this paper, the dynamic vibration response of sandwich beams with an anti-tetra-chiral lattice as a lightweight sandwiched core was studied by using a nonlinear finite element analysis (FEA). Also, the response was predicted by using the Rayleigh-Ritz method, assuming that the sandwich beam is composed of composite continuum materials with equivalent Young's modulus and shear modulus. Theoretical equations for these modules have already been reported by oher researchers, but the influence of beam geometries on these modules has not been clarified. In our calculation, the equivalent of these modules were caluclated by FEA for a 3-point bending model. In particular, it is found that the equivalent shear modulus depend significantly on the aslect ratio (length-to-thickness ratio L/h) of a beam. Also the prediction of the natural frequency of the beam obtained by the Rayleigh-Ritz method agrees well with FE results. Since a chical-cored sandwich beam can be easily fabricated by a 3D printer, the vibration response can be designed by changing the micro-architecture of the beam. In our study, two kinds of chiral-cored sandwich beams were manufactured by our in-house 3D printer, and its vibration response was measured by experiment. The observed eigenfrequency showed a similar trend to the prediction, but with quantitative errors, which is due to the several close vibration modes found in a particular frequency as well as the gemetrical imperfecition existed in a real specimen.

REFERENCES

[1] Mousanezhad, D., Haghpanah, B., Ghosh, R., Hamouda, A. M., Nayeb-Hashemi, H. and Vaziri, A. *Elastic properties of chiral, anti-chiral, and hierarchiral honeycombs: A simple energy-based approach.* Theoretical and Applied Mechanics Letters, **6**, 81-96 (2016)

[2] Wu, W., Hu, W., Qian, G., Liao, H., Xu, X., and Berto, F. *Mechanical design and multi-functional application of chiral mechanical metamaterials: A review.* Materials and Design, **180**, 107950 (2019).

[3] Spadoni, A., Ruzzene, R., and Scarpa, F. *Dynamic response of chiral truss-core assemblies.* Journal of intelligent material systems and structures, **17**, 941-952 (2006).

[4] Yamashita, S., Ohsawa, Isamu., Matsuo, Tsuyoshi., Zhang, Xin. and Takahashi, J. *Evaluation of young ' s modulus and out-of-plate shear modulus of carbon fiber reinforced thermoplastics by three point bending test.* Japan society for composite materials, **39**, 221-230 (2013).

[5] Fasana, A. and Marchesiello, S. *Rayleigh-Ritz analysis of sandwich beams.* Jounal of sound and vibration, **241**(4), 643-652(2001).